ULTRASTRUCTURE AND EARLY EMBRYONIC SHELL FORMATION IN THE TERRESTRIAL PULMONATE SNAIL, *EUHADRA HICKONIS*

S. TAKAICHI[1,6], V. MIZUHIRA[2], H. HASEGAWA[3], T. SUZAKI[4], M. NOTOYA[3], S. EJIRI[5], H. OZAWA[5] AND J. H. VAN WYK[6]

[1]*Laboratory of Electron Microscopy, National Cardiovascular Center Research Institute, 5-7-1 Fujishiro-dai, Suita, Osaka 565-0873, Japan;* [2]*Department of Cell Biology, Medical Research Institute, Tokyo Medical and Dental University, Bunkyo-ku, Tokyo 113-0034, Japan;* [3]*Developmental Research Laboratories, Shionogi & Co., Ltd, Toyonaka, Osaka 561-0825, Japan;* [4]*Department of Biology, Kobe University, Nada-ku, Kobe, 657-0013, Japan;* [5]*Department of Oral Anatomy, Niigata University School of Dentistry, Niigata 951-8126, Japan; and* [6]*Department of Zoology, University of Stellenbosch, Stellenbosch, 7600, South Africa*

(Received 30 June 2002; accepted 15 January 2003)

ABSTRACT

The distribution of calcium ion (Ca-ion) was demonstrated in the mantle epithelial cells by means of two-step chemical precipitation of Ca-ion in the pulmonate snail, *Euhadra hickonis*. K-oxalate/K-antimonate chemical replacement was done using a simultaneous computerized microwave-stimulated fixation method. These precipitates in the mantle epithelial cells were studied by electron-probe X-ray microanalysis (EDX) and electron energy-filtered imaging (EFI). The calculated values of the essential-elemental X-ray pulse ratios, which were obtained by computerized EDX analysis, agreed with those of the standard samples and theoretical values of Ca-antimonate. Typical EFI images and spectra energy of Ca and Sb were obtained from the surface mantle epithelial cells in the same tissue block as that used for EDX analysis where the elemental distribution of Ca and Sb was the same. The Ca-antimonate precipitates were formed in the intercellular space, vesicles and microvilli of mantle cells. In day 13 embryos, the columella and peripheral area were almost calcified, but in the dorsal area, Ca was still in the ionic state; the binding ratio of the former case was Ca:Sb = 1:0, that of the latter was Ca:Sb = 1:2, and that of the small intermediate area was Ca:Sb = 1:1.4. After day 17, the embryonal periostracum was almost calcified. Between days 15 and 20, strong Ca^{2+}-ATPase and carbonic anhydrase (CAHase) enzymatic activities were observed at the sites where Ca-ion was observed; intercellular spaces, vacuoles in the mantle cells, periostracum and homogeneous layer between the periostracum and mantle cell, and in the mitochondria. Ca^{2+}-ATPase may play important roles in the transportation of Ca-ion from the basal cell layer to the surface layer of the mantle cells and CAHase may play important roles in the chemical binding of Ca-ion and carbonate ion to produce calcium carbonate crystals in the newly developing embryonal shell.

INTRODUCTION

Most molluscs are known to secrete external calcareous shells that consist of organic and inorganic crystalline compounds (Wilbur & Saleuddin, 1983; Eyster, 1983, 1986). Although shell formation begins during early embryogenesis, most studies have described shell structure in juveniles and adults only (Kniprath, 1981; Eyster, 1983, 1986; Bielefeld, Peters & Becker, 1993; Hasse, Ehrenberg, Marxen, Becker & Epple, 2000). Studies dealing with early shell mineralization are rare and more studies are needed to document the degree to which the timing of initial shell mineralization varies among species (Eyster, 1986).

Shell formation during embryogenesis is characterized by a portion of the embryonic ectoderm, the so-called 'shell-field', temporarily invaginating, only to evaginate later (Eyster, 1986). During development the shell-field cells multiply and spread over a large portion of the embryonic surface (Kniprath, 1979). Although the cells of the shell-field invagination (SFI, shell-gland) were believed to be responsible for initial shell formation, recent ultrastructural studies on bivalves and gastropods have suggested that the SFI cells may not secrete the initial organic shell material (Eyster, 1983, 1985, 1986). Evidence seems to suggest that it is the cells lying immediately outside the SFI that secrete the first organic shell material (Eyster, 1986). Conflicting data have been reported in the literature regarding the role of the SFI cells in the early mineralization of the initial shell (Fretter & Pilkington, 1971; Kniprath, 1981; Eyster, 1986), but an ultrastructural study by Eyster (1986) suggested that the SFI is present during shell mineralization and may therefore be involved.

The shells of terrestrial gastropods are known to be mainly composed of calcium carbonate (Boer & Witteveen, 1980; Chetail & Krampitz, 1982). Little is known however about the elemental composition of shells of molluscs prior to metamorphosis (Eyster, 1986). Recently, Hasse *et al.* (2000) showed that the main component of the shell of the adult freshwater snail, *Biomphalaria glabrata*, was aragonite and that aragonite structures were already present in X-ray amorphous samples of 72-h-old eggs. Since it is not always possible to determine with light microscopy whether embryonic shells are mineralized, more detailed ultrastructural studies are needed describing initial shell mineralization relative to the developmental stage. Moreover, analytical techniques to detect tissue mineralization, specifically calcium deposition, need greater refinement. Hasse *et al.* (2000) employed high-resolution synchrotron X-ray powder diffractometry and X-ray absorption spectroscopy to study crystallinity during early shell formation in the freshwater snail, *Biomphalaria glabrata*. Bielefeld & Becker (1991) and Bielefeld, Zierold, Kortje & Becker (1992) employed various electron microscopic techniques to investigate the shell-forming tissue in *Biomphalaria glabrata*. These authors observed calcium precipitates using a tannic acid-antimonate technique in chemically fixed tissue. This method is similar to

Correspondence: J. H. van Wyk; e-mail: jhvw@sun.ac.za

that of Legato & Langer (1969), including potassium antimonate to precipitate Ca-ions. However, the reaction may also result in the precipitation of Na, Mg, Zn, and other ions or proteins other than Ca-ions. Thus, this method is not always reliable using electron microscope X-ray diffraction analyses (Mizuhira & Hasegawa, 1997). Improvement of the methods for detection of chemical precipitation of Ca-ions in the outer mantle epithelium are offered by Borgers, de Brabander, van Reempts, Awavoters & Jacob (1977), Ohara, Wada & Lieberman (1979), Borgers (1981), Borgers, Thone, Verheyen & Keurs (1984) and Mata, Staple & Fink (1987). Further refinements in the fixation and detection of Ca-ions were proposed by Mizuhira and co-workers (for reviews see Mizuhira, Hasegawa & Notoya, 1997, 1998; Hasegawa, Mizuhira & Notoya, 2000).

This paper describes the formation of the embryonic shell in the Japanese pulmonate snail, *Euhadra hickonis*, as observed using chemical fixation techniques for Ca-ions, and the elemental distribution in the shell by Energy Dispersive X-ray analysis (EDX) and Electron Energy-filtered Imaging (EFI). Shell calcification was investigated using: ultrastructural studies; Ca-ion localization during calcification (by EDX and EFI elemental analysis), and localization of enzymatic activities associated with shell calcification.

MATERIALS AND METHODS

Conventional light and electron microscopy

Fertilized eggs (5–20 days after laying) of *Euhadra hickonis* were obtained by opening each eggshell under a stereo zoom microscope. These embryonic cells were immersed in fixative containing 2% paraformaldehyde, 0.5% glutaraldehyde, 0.1% tannic acid, 2 mM $CaCl_2$ and 1 mM $MgCl_2$ in a 0.1 M cacodylate buffer (pH 7.2). The tissues in the fixative were then microwave-irradiated (MWI; 500 W) in a water-bath for about 30 s at room temperature (Notoya, Hasegawa & Mizuhira, 1990; Mizuhira *et al.*, 1997, 1998). After the irradiation, these samples were left in the same fixative for about 60 min at room temperature. Tissue samples were then washed several times with 0.1 M cacodylate buffer and postfixed with 1% osmium tetroxide for 2 h at room temperature. The specimens were washed with 0.1% sodium acetate, stained *en bloc* with 2% uranyl acetate for 40 min, washed again with 0.1% sodium acetate, dehydrated through a graded ethanol series, and finally embedded in Spurr's low viscosity resin (Spurr, 1969).

For light microscopy, tissues were sectioned at approximately 0.5 μm using glass knives and stained with toluidine blue solution (Bancroft & Stevens, 1977). For transmission electron microscopy (TEM), tissues were trimmed further, ultrathin sections taken and stained with 3% uranyl acetate in 30% ethanol, followed by treatment with Reynold's lead citrate. Sections were examined under a Hitachi H-600 electron microscope operating at 100 kV.

Ca-ion detection by computerized EDX analysis

To detect Ca-ion in embryonic cells of *Euhadra hickonis*, the methods of Mizuhira *et al.* (1997, 1998) and Hasegawa *et al.* (2000) were used. Between days 5–22 after spawning, the eggs were removed to detect Ca-ions and immersed in fixative containing 2% paraformaldehyde, 0.5% glutaraldehyde, 0.1% tannic acid and 60 mM potassium (K) oxalate in a 0.1 M cacodylate buffer (pH 7.2), and subsequently processed as described above. Unstained ultrathin sections were picked up on nylon grids and coated with carbon. They were then observed by conventional electron microscopy under a JEM 1200EX transmission electron microscope (JEOL, Japan). EDX analysis was done with an electron microscope fitted with an EDAX-PV-9800 (Japan Philips), and a microcomputer analysing system, using SEM and STEM mode apparatus with an accelerating voltage of 60 kV.

In this study we used a sensitive method for detecting calcium in biological tissues, the 'replacement' method, in which calcium oxalate in the cells and tissues is changed to calcium antimonate (Ca•Sb) by antimonic acid (see Mizuhira *et al.*, 1997; Hasegawa *et al.*, 2000). The essential-elemental X-ray pulses of calcium and antimony were counted for 200 s in a selected area (100 × 200 μm^2) in the STEM mode. EDX analysis was performed after strict calibration of the X-ray detection (Mizuhira *et al.*, 1997, 1998), which began with semiautomatic calibration for 60 min followed by examination of Cu•Kα and Si•Kα; Sb•Lα and Ca•Kα as standard analysing samples. The results from the EDX-detector were checked by careful operation using basic manipulation methods. In the final step, crystal powders of KCl, $K[Sb(OH)_6]_2$ and $Ca[Sb(OH)_6]_2$ were analysed as in the standard samples. The calibration was done until the measured values coincided with the theoretical values. Thereafter, the samples were analysed by computerized EDX.

Ca-ion detection under electron energy-filtered imaging (EFI)

In EFI analysis, the same samples were used as in the EDX analysis. Super-ultrathin sections (less than 50 nm, mostly 30 nm in thickness) were mounted on 400-mesh copper grids. Unstained, uncoated ultrathin sections were analysed by electron energy-loss spectroscopy (EELS) and electron spectroscopic imaging using a ZEISS EM-902A operating at 80 kV. The peaks of electron energy spectra of the $Ca•L_{2,3}$ (355 eV) and $Sb•M_{4,5}$ (570 eV) were confirmed by the EFI (Nakahara & Bevelander, 1971; Mizuhira *et al.*, 1997, 1998). Each chemical element was detected as a digital image of the net EF·image CEM-902A (IBAS). The data of the digital image were obtained by computer after each background image was subtracted.

Distribution of Ca^{2+}-ATPase enzymatic activity

Snail eggshells were broken under a stereomicroscope, and unhatched embryos collected. The embryos were subsequently prefixed in 2% paraformaldehyde, 0.5% glutaraldehyde in a 0.1 M cacodylate buffer (pH 7.2), then microwaved at 15°C using a computer-controlled 'intermittent' irradiation schedule. These specimens were rinsed several times with buffered solution. Fixed tissue blocks were immersed in incubation medium (Fujimoto & Ogawa, 1982). Specimens were postfixed with 1% OsO_4, dehydrated in an ethanol series and embedded in Spurr's resin. Ultrathin sections were mounted on copper grids, double electron-stained with microwave irradiation (MWI; Hasegawa, Mizuhira & Notoya, 1991; Mizuhira, Hasegawa & Notoya, 1993, 1994), and examined under a Hitachi H-600 or JEM 1200EX (JEOL, Japan) electron microscope. As a control experiment, calcium was omitted from the incubation medium.

Demonstration of enzymatic activities of carbonic anhydrase in shell formation

The developing embryonic cells were prefixed in the same fixative as above with the intermittent irradiation method. The fixed specimens were rinsed with 0.1 M cacodylate buffer containing 0.25 M saccharose at room temperature. The specimens were floated in Hansson's incubation medium for about 20 min at room temperature (Hansson, 1967). In the control experiment, specimens were preincubated in 10–4 M acetozolamide containing 0.02 mM saccharose solution for 20 min before being floated in the incubation medium. Specimens must be floated to keep them aerated and moist. Following the removal from the solution, specimens were rinsed with 0.1 M cacodylate buffer and immersed in 0.2% lead citrate for 20–30 min at room tempera-

ture. The treated specimens were rinsed with 0.1 M cacodylate buffer several times, postfixed with 1 % OsO4, dehydrated in an ethanol series and embedded in Spurr's resin. Ultrathin sections (70–80 nm thickness) were stained with double electron staining with MWI (Hasegawa *et al.*, 1991; Mizuhira *et al.*, 1993, 1994). Sections were examined under a Hitachi H-600 or JEM 1200EX electron microscope

RESULTS

General observations (Fig. 1)

Euhadra hickonis produced eggs from the middle of March to the end of June. The colour of the eggs is milky white with a diameter of about 2 mm and 50–60 eggs are laid at once. The eggs hatched at about 30 days after spawning. Initial shell formation was observed in day 13 embryos (Fig. 1), reaching completion around days 19–20 following spawning. The shell is formed by secretory activity in the outer mantle epithelial cells. The shell-gland primordium first appears in the region of the periostracum groove, on the dorsal side in day 13 embryos. During days 14–16 after spawning the periostracum elongates towards the surface of the dorsal side and the periostracum extends into the lumen of the mantle cavity. During days 17–18, the embryonic body is surrounded by the periostracum (the outer mantle epithelium closely connected with the shell formation).

Light microscopic observations (Figs 2–5)

Initiation of shell formation was confirmed in day 13 embryos (Fig. 2: arrow: toluidine-stained section, 0.5–1 μm). During shell formation, the outer mantle epithelial cells line up along the basement membrane. The surface of the outer mantle epithelial cells is covered with microvilli, while the intracellular areas contain cytoplasmic organelles. Another feature of these sections is that two types of invaginations, type-A and type-B, were evident (Fig. 2). Type-A invaginations continue forward from the columella of the shell, while type-B invaginations develop into the mantle cavity and yolk granules (Fig. 2). The ciliated ventral epithelium (VE) and periostracal groove (PG: arrowhead) surround the columella area (Type-A invagination; Fig. 3). A ventral concavity containing calcareous material is present between the dorsal epithelium (DE) and ventral region. The developing periostracum was observed in close proximity to the dorsal epithelium (DE). The periostracum of the mantle cavity (MC) area (Type-B invaginations) is not fully formed in the day 13 embryos (Fig. 4: arrowheads). However, the day 20 embryo is covered with a shell (Fig. 5: arrowheads) and the other organs are fully developed.

X-ray microanalysis (Figs 6–14)

At the beginning of this study, we examined a calcium antimonate (Ca-antimonate) standard (crystal powder) using a computerized EDX system (Philips Japan, EDAX-9800; Fig. 6). Theoretical calculation values of the atomic binding ratio (AT%) of Ca-antimonate is Ca:Sb = 1:2, and molecular weight ratio (WT%) is Ca (40.08):Sb (121.7 × 2) = 14.1 : 85.9. Analysed data show AT%, Ca:Sb (1:2) = 33.5:66.5, and WT%, Ca:Sb (14.1:85.9) = 14.2:85.8 (Fig. 6).

EDX analysis of the day 10 embryos (Fig. 7)

In day 10 embryos, fine electron-opaque precipitates (arrowheads) could be observed on the apical membrane of the mantle epithelial cells (Fig. 7A). However, judging by the atomic binding ratio (AT%; Ca:Sb = 2:98) and the elemental molecular weight ratio (WT%; Ca:Sb = 7:93) (Fig. 7B), these small precipitates mostly contained antimony only, with little or no calcium.

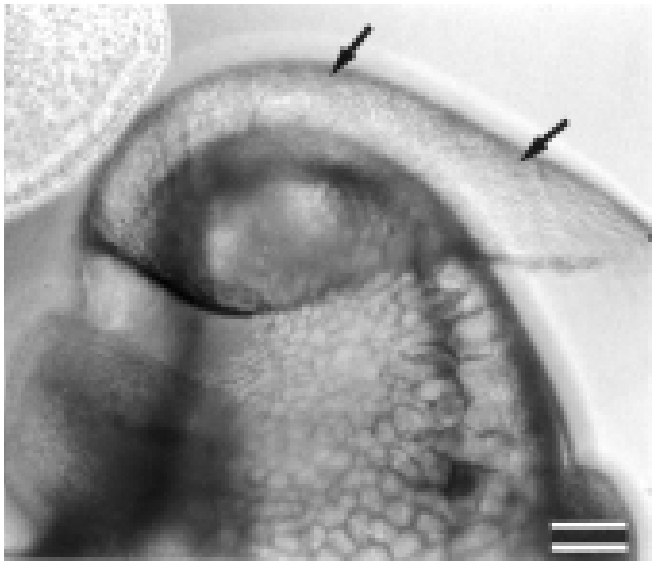

Figure 1. Early shell formation in the day 13 embryo of *Euhadra hickonis*. Note that the heart is covered with a very thin shell (arrows). Scale bar = 25 μm.

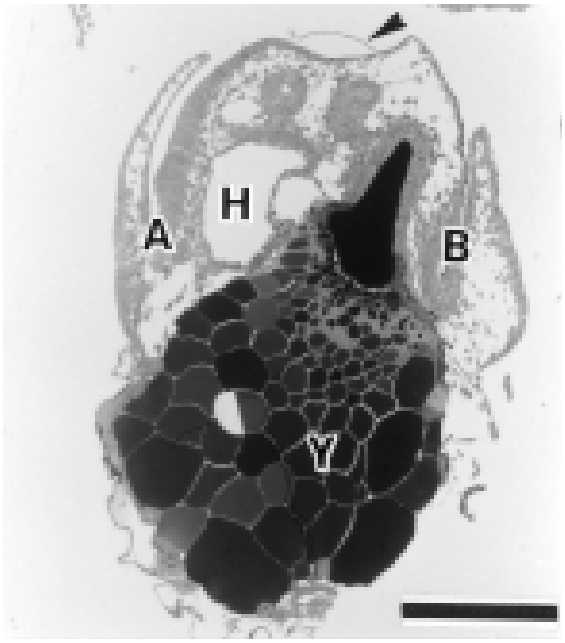

Figure 2. The day 13 embryo of *Euhadra hickonis*: two parts of the invagination, invagination A of the elongated columella; invagination B in the area of mantle cavities. Arrowhead indicates shell. Y, yolk granules; H, heart. Scale bar = 25 μm.

Precipitates were observed in the cellular cytoplasm (Fig. 7A), similar to the surface precipitates, likewise only containing antimony and little calcium.

EDX analysis of the day 13 embryos (Figs 8–14)

The columellar area. In the columellar area the first calcification activity was observed, with evidence of Ca-ions being transformed to calcium carbonate during the calcification process (Fig. 8A–C). The bifurcated periostracum consists of two parts: one is the periostracal groove compartment and the other is the spherical shape containing homogeneous electron-dense material, which is already surrounded by the periostracum (Fig. 8A). These

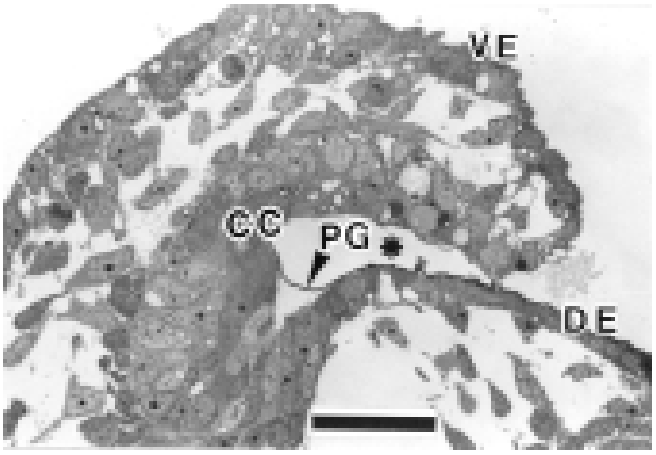

Figure 3. The columellar area (invagination A) of the day 13 embryo of *Euhadra hickonis*. Note the ciliated ventral epithelium (VE), periostracum groove (PG: arrowhead), columella cockleae (CC), dorsal epithelium (DE) and deep periostracal groove area filled with calcareous materials (*). Scale bar = 5 μm.

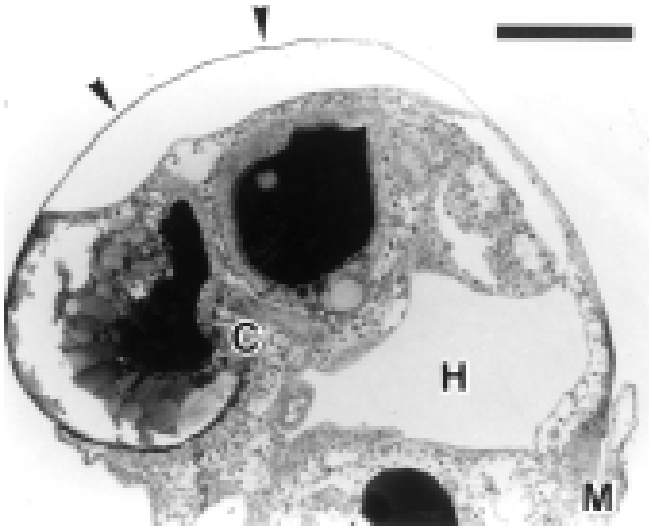

Figure 5. The day 20 embryo of *Euhadra hickonis*. The embryonic shell is completely formed. Arowheads indicate shell. C, columella; M, mantle cavity; H, heart. Scale bar = 25 μm.

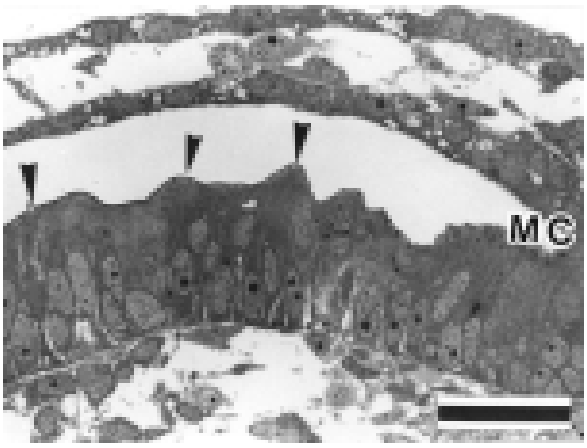

Figure 4. The mantle cavity (MC) area (invagination B) of the day 13 embryo of *Euhadra hickonis*. The periostracum is not completely formed. Arrowheads indicate periostracum. Scale bar = 5 μm.

precipitated materials are completely calcified (Fig. 8A: arrowheads; Fig. 8B, C). Indications were that these precipitates are calcium carbonate. In this precipitated material only Ca•$K_{a,b}$ was detected, and no Sb was detected. The binding ratio of Ca:Sb was 1:0 (Fig. 8C: EDX spectrum and see Fig. 13:I). Under a common EDX analysis, Carbon (C•K) was not detected; only Ca•K could be detected.

The periostracum, the mantle outer epithelial intercellular space, and cell interior. In the day 13 embryo, the periostracum (0.25 μm in width), is located on the surface of the outer epithelial cells of the mantle (Fig. 9). Electron-opaque plug-like or prismatic ultrastructures (0.5–1.5 μm in width) were observed beneath the periostracum mantle of the outer epithelial cells (Fig. 9: arrowheads and insert). These structural materials are exhibited only in the early stages of embryonic shell formation and cannot be recognized using conventional methods; they are only observed when the K-oxalate/K-antimonate/MWI fixation method is used. An abundance of precipitated deposits (Fig. 9: arrows) were recognized in the intercellular spaces between the underlying

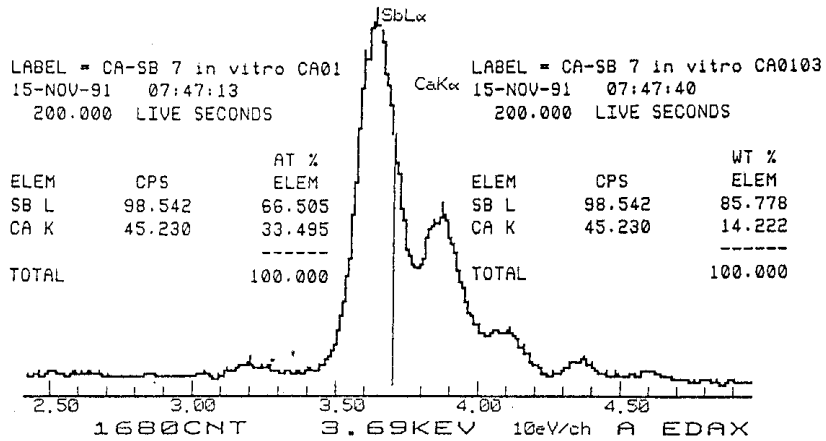

Figure 6. A typical EDX-spectrum obtained from crystal of calcium antimonate. Calcium antimonate standard sample analysed under computerized EDX (Philips Japan, EDAX-9800). Calculated values of atomic binding ratio (AT%) and molecular weight ratio (WT%) in both Ca and Sb were the same as theoretical values.

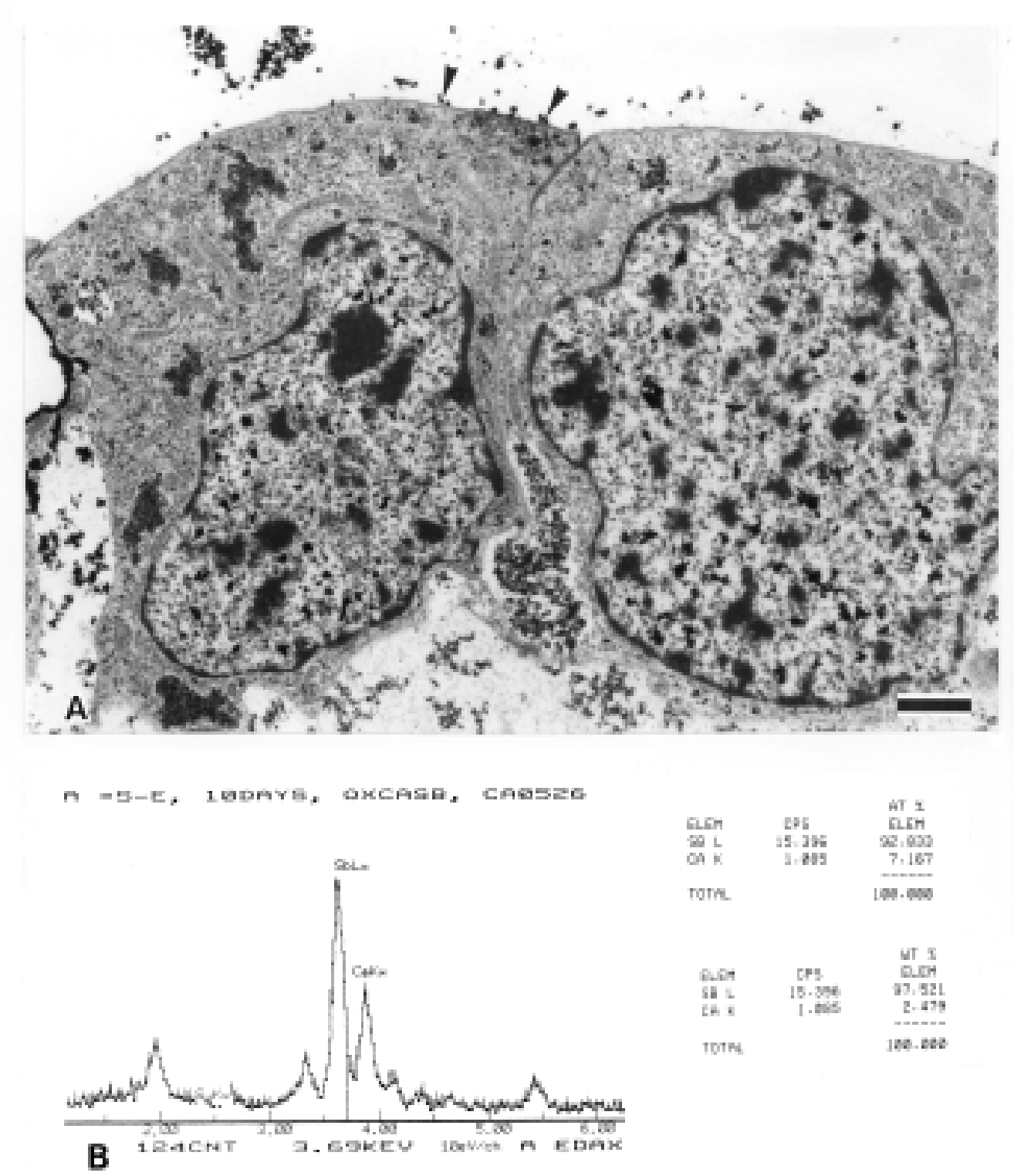

Figure 7. An electron micrograph of the day 10 embryo of *Euhadra hickonis* (**A**). Small precipitates are seen on the mantle epithelial cell (arrowheads). Scale bar = 1 μm. These precipitates do not contain calcium ion, as shown in the EDX spectrum (**B**).

mantle cells, in the intercellular junctional complexes and microvilli on the apical surfaces of the mantle cells adjacent to the ventral aspects of the periostracum (septate junction).

Cytochemical analyses (Fig. 10) of the plug-like prismatic structural material beneath the periostracum, the precipitates in the intercellular spaces (Fig. 9: arrows) and the septate junctional area, indicated the ratio Ca:Sb = 1:2 (AT%; 34.0:66.0 and WT%; 14.5:85.5, EDX spectrum; Fig. 10). The EDX-analysis signifies that it is equal to the calculated theoretical value of Ca:antimonate: ($Ca[Sb(OH)_6]_2$). Therefore, Ca-ion and antimonic acid $[Sb(OH)_6]^-$ exist in the ratio 1:2, which suggests that they exist as an ionic state and yet in a calcified state. This observa-

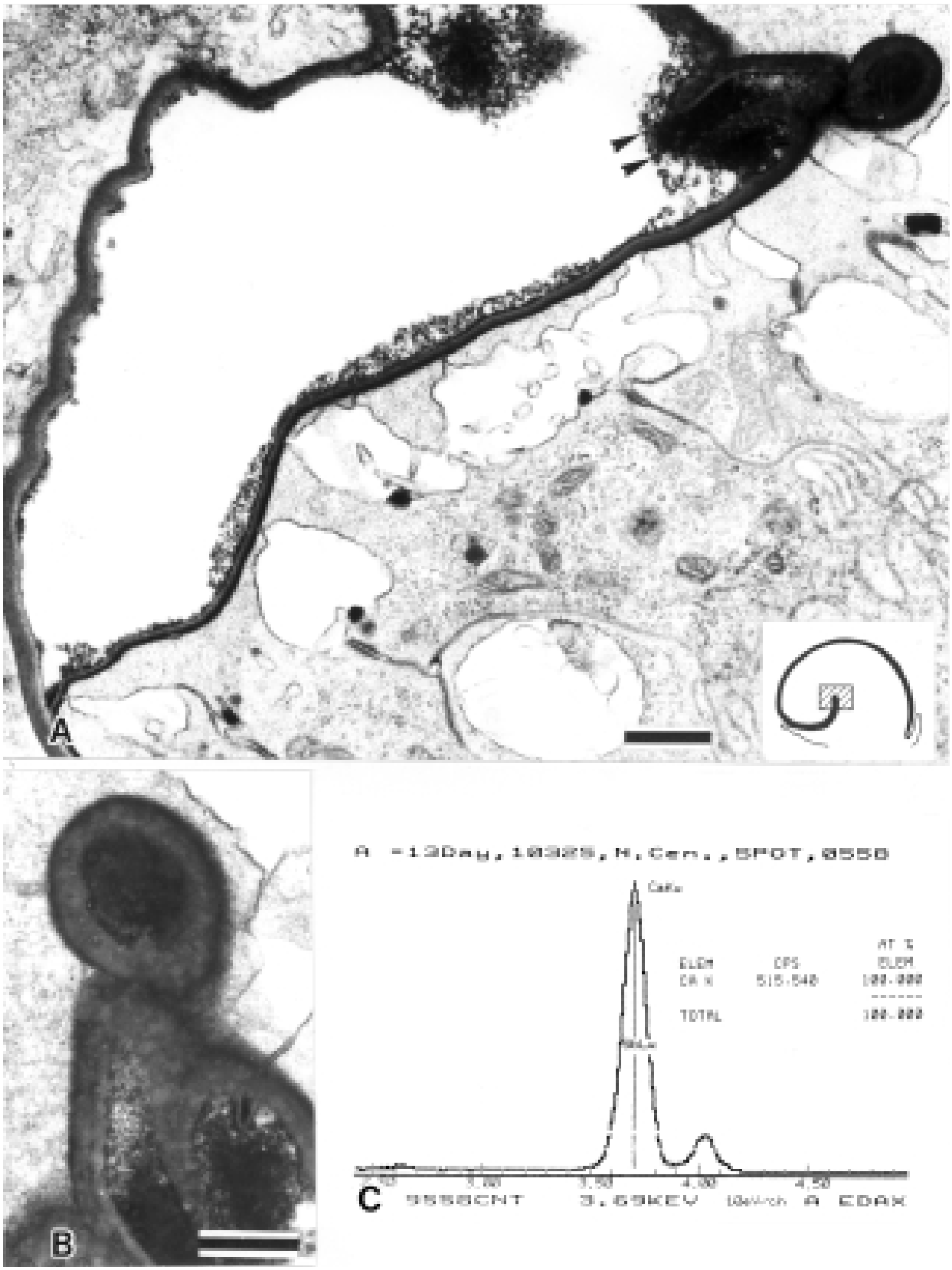

Figure 8. Electron micrographs of the columella area in the day 10 embryo of *Euhadra hickonis*. The precipitated dense materials (arrowheads) are detected as Ca•$K_{a, b}$ only; Sb is not detected. The binding ratios of Ca:Sb = 1:0 (Fig. 8C). Scale bars: **A** = 1 μm; **B** = 500 nm.

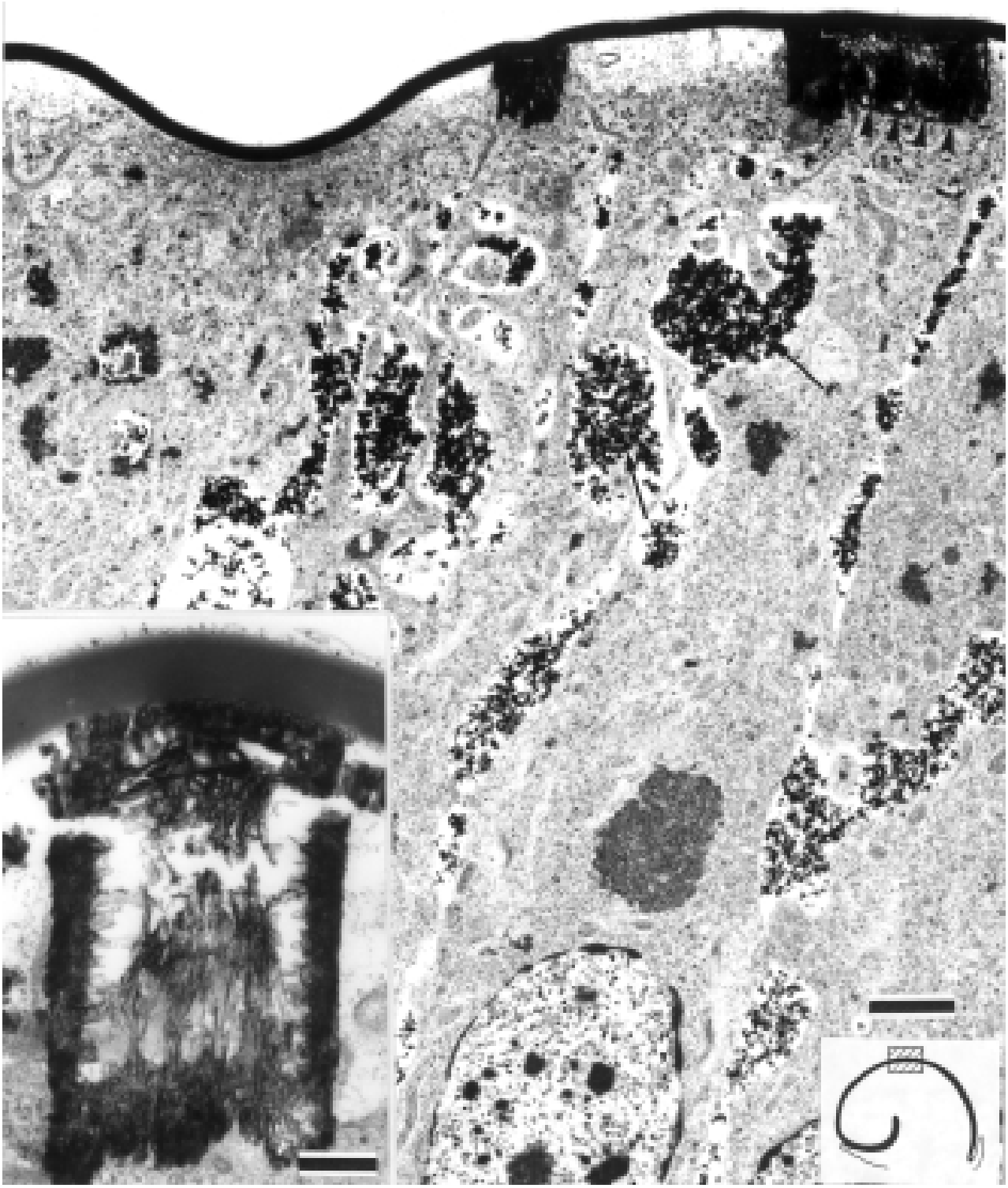

Figure 9. The day 13 embryo of *Euhadra hickonis*. The use of the K-oxalate/K-antimonate/MWI chemical method is shown to result in a characteristic ultrastructure, which is the electron-opaque plug-like (insert) or prismatic structure, 0.5–1.5 μm in width, formed beneath the periostracum mantle outer epithelial cells. The precipitated deposits (arrows) are recognized in the intercellular space, junctional complex and microvilli, but mitochondria contain few precipitates. Scale bar = 2 μm; scale bar of insert = 250 nm.

tion suggests that these precipitated masses were formed during the transformation of Ca-ions into the crystal structure of calcium carbonate. The fine prismatic calcium crystal structures represent the precursor material of embryonic shell. With the advance of calcification, these precipitated materials cannot be detected as Ca-antimonate by the EDX analysis, but can only be recognized as pure $Ca•K_{a,b}$

The yolk area. A great number of yolk granules exist in the peripheral region of the columellar zone. A linear structure showing

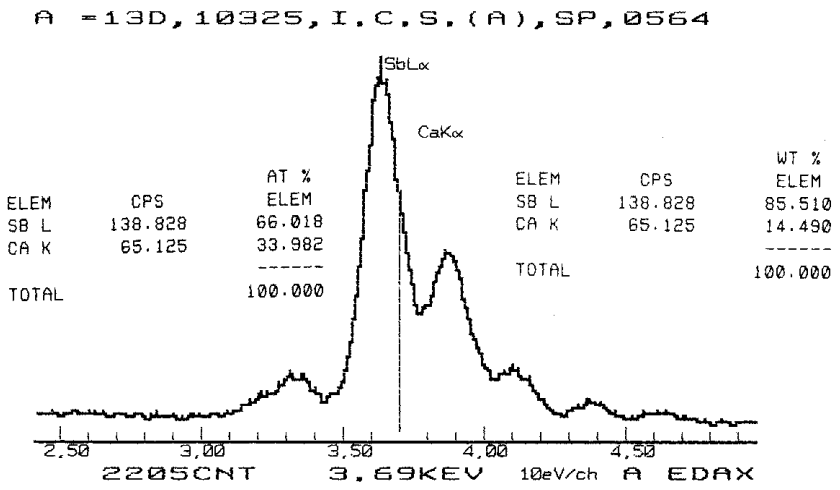

Figure 10. Cytochemically fine precipitates in the intercellular space (Fig. 9: arrows) and the plug-like prismatic structural material are shown to be Ca:Sb = 1:2 (AT%; 34.0 : 66.0 and WT%; 14.5:85.5).

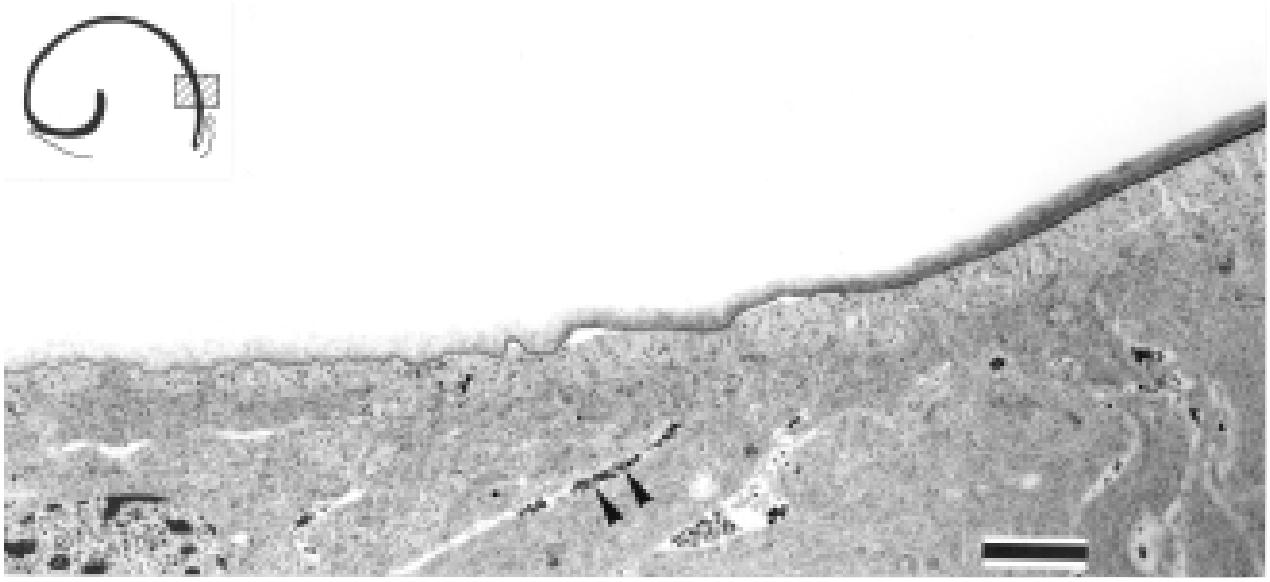

Figure 11. The fine precipitates observed in the intercellular space (arrowheads) in the mantle cavity. These precipitates are Ca-ion, the ratio of atomic binding (AT%) of Ca:Sb = 1:2 by the EDX analysis (see Fig. 13). Scale bar = 2 μm.

abundant precipitates is evident between the yolk granules. The EDX analysis data indicated that Ca-ions exist as a calcium antimonate precipitate. The theoretical ratio of atomic binding of calcium antimonate is Ca:Sb = 1:2, and we obtained the same ratio from the Ca-antimonate standard during the EDX analysis (data not shown). This means that the Ca-ions exist and are stored in an ionic state.

Mantle cavity. A great number of precipitates can be seen on the outer faces of cellular microvilli and in the mantle cavity (Figs 11 and 12). The EDX analysis indicates that the ratio of atomic binding of calcium antimonate of these precipitates is Ca:Sb = 1:2, suggesting that calcium exists in an ionic state.

Regional comparison. During the process of calcification, the Ca-ions (precipitates) in the cellular interior decrease markedly in the day 22 embryo to the point of almost disappearing. In such conditions, the ratios between the $Ca{\bullet}K_{a,\,b}$ increase rapidly and, in content, the antimony decreases rapidly in accordance with the theoretical values calculated by the EDX-analysis (see Fig. 6). These phenomena indicate that the calcification process has progressed rapidly.

Figure 13 summarizes the calcification process of the day 13 embryo under the EDX-analysis. The columella area (Fig. 13:I) is already calcified, and the calculated theoretical values are shown to be calcium only: Ca:Sb = 1:0. The X-ray energy spectrum of $Ca{\bullet}K_{a,b,}$ as analysed by EDX, point to an adjacent area of the columella area in the developmental stages of calcification. Its calculated value is shown to be Ca:Sb = 1:1.4 (Fig.13:II). The dorsal mantle epithelial area is still almost in a Ca-ion state, binding with antimonic acid, Ca:Sb = 1:2 (Fig. 13:III). Figure 14 shows the mantle epithelial cells (A, A', A''), intercellular space (B), and columella area (C) of the proceeding calcification of the days 10, 13 and 22 embryos. The precipitates of the mantle epithelial cell

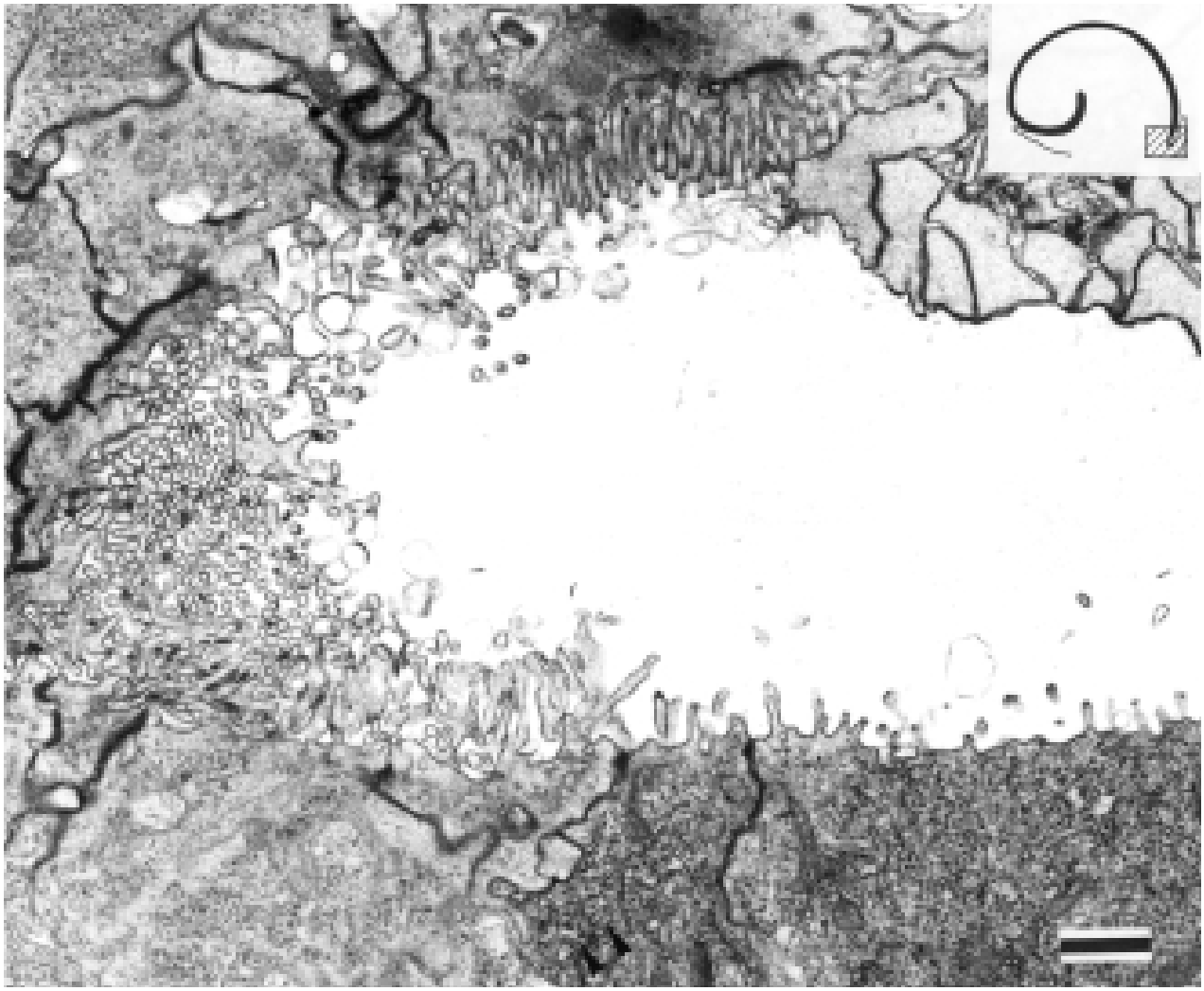

Figure 12. The fine precipitates observed in the outer faces of the cellular microvilli in the mantle cavity. As in Figure 11, these precipitates are Ca-ion (see Fig. 13). Scale bar = 1 μm.

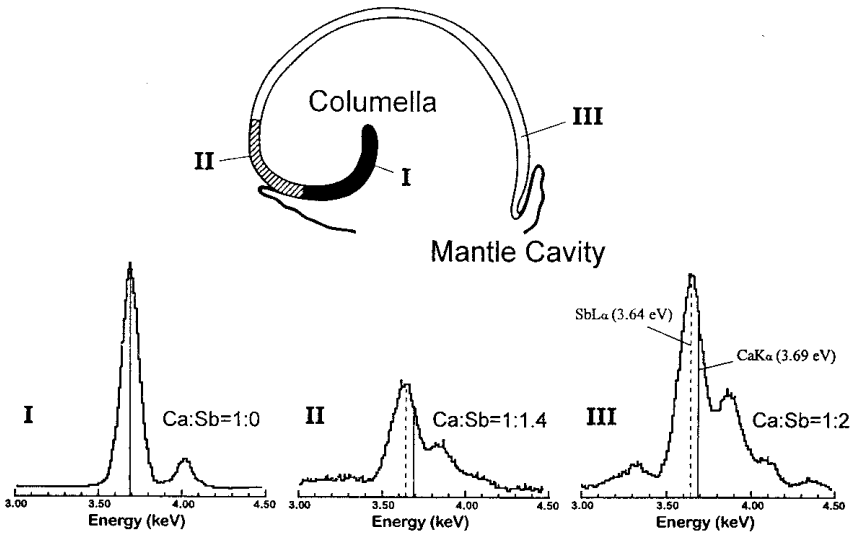

Figure 13. A schematic summary of the calcification process as seen in the day 13 embryo of *Euhadra hickonis* employing EDX-analysis. The columellar (I) is already calcified. The ratio of atomic binding (AT%) of Ca:Sb = 1:0. Dorsal, mantle epithelial area (III), Ca:Sb = 1:2. Between columella and dorsal area (II), Ca:Sb = 1:1.4.

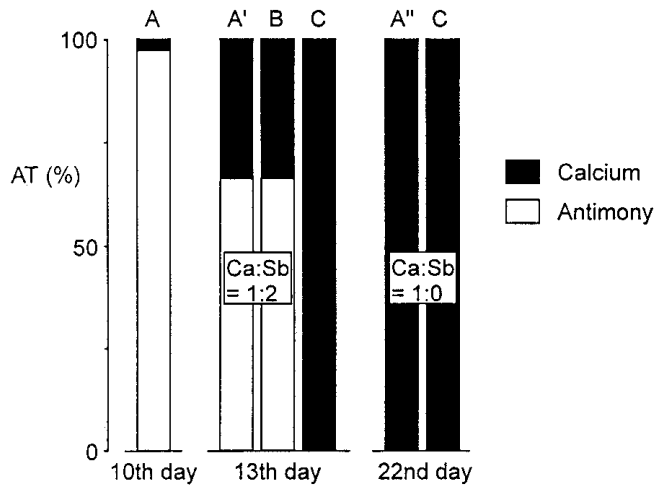

Figure 14. Progression of calcification in the embryonic shell of *Euhadra hickonis*. The mantle epithelial cells (A, A′, A″), intercellular space (B) and columellar area (C) of calcification in the days 10, 13 and 22 embryos. The precipitates of cell surface membrane (A) in the day 10 embryo do not show the Ca-ion. In the day 13 embryo, Ca-ions are clearly visible. The collumellar area (C) is made up only of Ca-ion. The surface membrane (A′) and inter-cellular space (B) are almost entirely in the Ca-ion state, binding with antimonic acid, Ca:Sb = 1:2 (AT%). In the day 22 embryo the columella area (C) and surface membrane (A'') are composed of calcium carbonate crystals Ca:Sb = 1:0 (AT%).

surface membrane in the day 10 embryos do not show Ca-ions. In the day 13 embryos, Ca-ions are recognized by EDX-analysis as an ionic state (Ca:Sb = 1:2, AT%). However, in the day 22 mantle epithelial cell surface is composed of calcium carbonate crystals (Ca:Sb = 1:0, AT%), and is already calcified.

Analysis by electron energy-filtered imaging (EFI) (Figs 15, 16)

For the analysis by EFI, we used the same tissue block used for the EDX. As shown in Figure 9 the very fine precipitates of Ca-antimonate were observed inside and outside of the mantle epithelial cells in the day 13 embryos. The digital EF-images are shown in Figure 15. The dark-field 250 eV EF-image is coloured with a blue-background with the white granules marking the Ca-antimonate precipitates (A). EFI of Ca•$L_{2,3}$ (355 eV:B) and Sb•$M_{4,5}$ (570 eV:C) images are colour-coded with sky blue (B) and light green (C), and are superimposed on the dark-field 250 eV image with a red background. From these data the precipitated deposits on the surface of mantle epithelial cells are calcium-antimonate that has passed through the cellular interior. The elemental electron energy-loss spectra of Ca•$L_{2,3}$ and Sb•$M_{4,5}$ were detected from these precipitates (Fig. 16).

The days 17 and 18 embryos represent almost completely calcified embryonic shells. Each organ is fully formed and the precipitates of Ca-antimonate have disappeared since being transformed into the calcium carbonate crystals during the calcification process (data not shown).

Localization and advance of Ca^{2+}-ATPase and carbonic anhydrase enzymatic activities (Figs 17–19)

The microvilli were stained intensely to observe the enzymatic activities of Ca^{2+}-ATPase (Fig. 17A–C) and carbonic anhydrase (CAHase: Fig. 18A–C) associated with either the transport of calcium, or transformation of calcium to calcium carbonate (Abolins-Krogis, 1986). Appearance of both enzymatic activities was observed in the same locations and at the same cellular stages. The level of enzymatic activities corresponded well with that of the Ca-ion transportation processes. No enzymatic activities were observed in the control tissues or cellular sites.

The localization of enzymatic activities was exhibited in the microvilli of the mantle and ventral epithelial cells (Fig. 17A: arrow; Fig. 18A,C), intercellular space (Fig. 17B: arrow; Fig. 18B), septate junction, mitochondrial cisternae (Fig. 17C: arrow), and peripheral area of periostracal groove area in the day 17–18 embryonic cells. These enzymatic activities were absent in the control tissues, early embryonic stages (days 10–13) and embryos older than 19 days. It was noteworthy that in the same area, but at different developmental stages, different processes may be observed by the different methods. In day 13 embryos, the EDX method showed the Ca-ions appearing. By days 17–18 of embryonic development strong enzymatic activities appeared in the same regions indicating Ca-ions.

The distribution of the Ca^{2+}-ATPase and CAHase enzymatic activities in the day 17 and day 18 embryos are schematically presented in Figure 19A. In the corresponding Figure 19B the cellular locations of Ca-ions in the day 13 embryos cells are shown. It is clear that there is a remarkable coincidence of cellular locations exhibiting enzymatic activity, pointing to calcium transport and calcification.

DISCUSSION

The role of the invaginated plate, the so-called 'shell field invagination' (SFI = shell-gland) (Kniprath, 1972, 1979, 1981; Saleuddin, 1975) in the initial shell secretion remains controversial. Initially, the cells of the SFI were generally believed to be responsible for initial shell formation (Fretter & Graham, 1962). Subsequent ultrastructural evidence from bivalves and gastropods (Kniprath, 1977, 1980, 1981; Eyster 1983), however, suggested that SFI cells do not secrete initial shell material, but rather that this emanate from shell-field cells lying immediately outside the invagination. Reports that the SFI disappears before the onset of initial shell mineralization support this conclusion (Kniprath, 1980; Eyster 1983). Contrary to these reports, Eyster (1986) presented ultrastructural evidence suggesting that in three gastropod species the cells of the SFI are still present and may play an active role in initial molluscan shell formation. Results from the present study support the proposal (Eyster, 1983, 1986) that calcium might be transported through cells lining the SFI to the SFI lumen and then to the inner surfaces of the newly formed shell.

The morphology of periostracum formation has been described in various studies (Eyster, 1983, 1986; Bielefeld & Becker, 1991; Bielefeld *et al.*, 1992, 1993; Ireland, 1991, 1993). The histology and histochemistry of the mantle edge of *Lymnaea stagnalis* at the light microscope level were reported by Timmermans (1969), whereas Kniprath (1972) studied the ultrastructural features of the cells in the mantle edge known to produce the periostracum and the outer layer of the shell in *L. stagnalis*. The process of calcification in the outer mantle edge gland was analysed with EDX and EF-spectrum (Kniprath, 1972; Boer & Witteveen, 1980; Jones & Davis, 1982; Mizuhira, 1989: Bielefeld & Becker, 1991; Bielefeld *et al.*, 1992, 1993; Ireland, 1993). Moreover, several inorganic chemical precipitation methods to detect Ca-ions in the embryonic shell formation raised some controversial points. The most important point is that the inorganic chemical precipitation methods for detecting the Ca-ions are not always reliable in both EDX and FI detection methods (Mizuhira *et al.*, 1997; Mizuhira *et al.*, 1998; Hasegawa *et al.*, 2000). Therefore, we followed the experimental methods of Mizuhira and coworkers, in both EDX analysis and EF digital imaging methods, followed by the two-step chemical precipitation techniques, once the reliability had been established. Using the Mizuhira methods we detected Ca-ions in the outer mantle epithelial cells in day 10

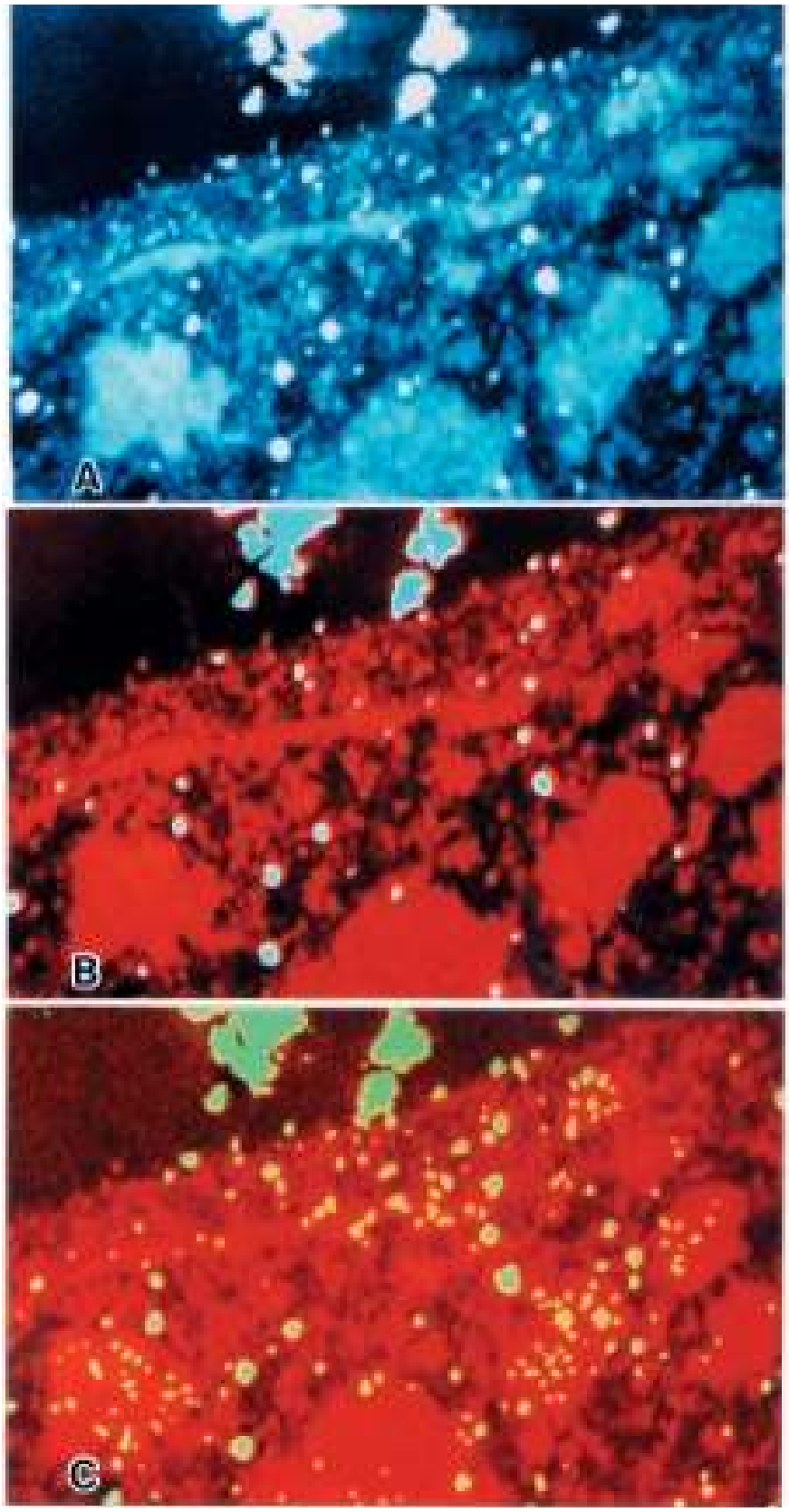

Figure 15. Super-ultrathin section, 30 nm thickness, of the mantle epithelial cells of the day 13 embryo of *Euhadra hickonis*, which was analysed with the help of electron energy-loss spectroscopy (EELS or EF) using a ZEISS EM-902A/CEM-902A/IP. Digital EF image (dark-field) shown in blue at 250 eV; white granules are precipitates of Ca-antimonate (**A**). The EF of Ca•$L_{2,3}$ (355 eV) image and Sb.$M_{4,5}$ (570 eV) image are colour coded with sky blue (**B**) and light green (**C**), and are superimposed on the dark-field image (red base).

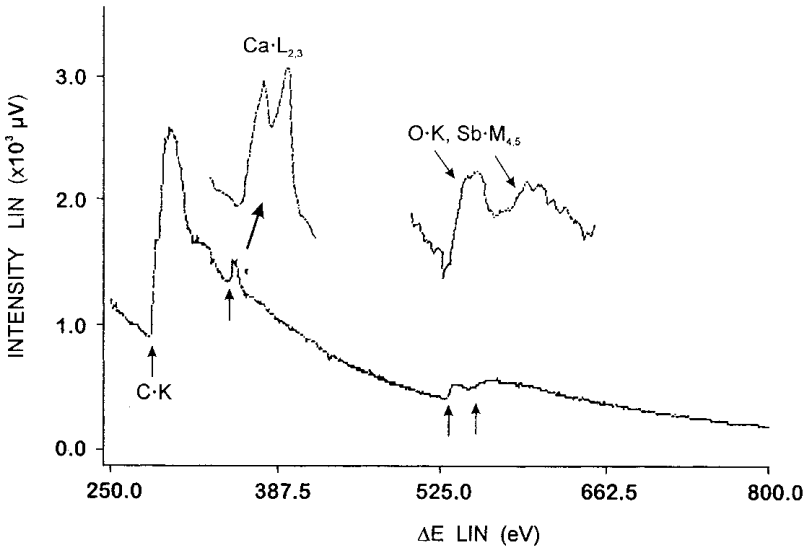

Figure 16. Digital EF spectrum obtained from the precipitate in a section. Ca•$L_{2,3}$, O•K and Sb•$M_{4,5}$ peaks are clear.

E. hickonis embryos. In the day 13 embryos the appearance of Ca-ions rapidly increased. With the progress of calcification, there are increasing Ca-ions (Ca•K_a), paralleled by a corresponding decrease in the detection of antimonic acid ions (Sb•L). We also recognized that the rate of appearance of Ca-ion and antimonic acid ion is remarkably different among several regions of the mantle epithelial cells of the day 13 embryo.

Evidently, in the present study, the fact that the calculation of the chemical reaction of calcium and antimonic acid ion corresponds with theoretical calculations, suggests that the methods of the Mizuhira and co-workers are dependable and estimates of Ca-ion density are accurate. To further substantiate this conclusion, we used ultrathin 30-nm sections, observed under an EELS (EF) electron microscope (Zeiss EM/CEN-902A/IBAS) at 80 kV accelerating voltage with an electrostatic prism/mirror/prism type energy filter (Niigata University). As shown in Figs 15A–C and 16, electron energy spectra of Ca•$L_{2,3}$, Sb•$M_{4,5}$ and O•K were obtained from the precipitates in the day 13 *E. hickonis* embryos.

The application of microwave-irradiation fixation combined with Ca-ion detection, and computerized EDX or EFI analyses, brings rapid and equal infiltration of the chemicals into the depths of the tissues, and make extremely fine and homogeneous reaction products in the tissue block. Clearly, superior fixation results, compared to the conventional immersion methods, were obtained by employing the microwave-irradiation methods of Mizuhira and co-workers (for reviews see Mizuhira *et al.*, 1997; 1998; Hasegawa *et al.*, 2000). We have demonstrated colour-coded net calcium EF digital images of Ca•L and Sb•M superimposed on the electron spectroscopic dark-field images at 250 eV. Ca•L and Sb•M net EF digital images were distributed on the same sites in the outer mantle epithelial cells in the day 13 embryos. The formation of calcified embryonic shell is closely related to the appearance and transport of the Ca-ion. Hasse *et al.* (2000) showed that the main component of the adult shell is aragonite and confirmed the presence of aragonitic structures in X-ray amorphous samples of 72 h in the freshwater snail, *Biomphalaria glabrata.* The involvement of the constituents of the organic matrix of the periostracum in the calcification process of the shell through controlling crystal nucleation and subsequent modification (Marxen, Hemmer, Gehrke & Becker, 1998) needs further study in *Euhadra hickonis.*

The localization of the Ca-ion is also associated with enzymatic activities. Ultrastructural localization of the related enzymatic activities of Ca-ion transport or calcification, the activities of Ca^{2+}-ATPase and carbonic anhydrase (CAHase) were observed in the mantle epithelial cell membranes, vesicles and mitochondria. The enhanced CAHase functional stage in *Euhadra hickonis* conforms to an initial stage of calcification; furthermore, the antimonic acid ion decreases in proportion to the increase of Ca-ion in these stages. In the present study, the enzymatic activity as observed in the epithelium on the basal lateral plasma membrane and concentrated in the microvilli is in accordance with the hypothesis that the mantle edge gland is not primarily involved in HCO_3^--secretion (Kniprath, 1997, 1980, 1981).

As the shell calcification proceeded, the antimonic acid ion was not detected, but the only Ca-ion was detected under the EDX. At the same time, the enzymatic activities disappeared on the completion of the calcification. The function of CAHase would be to enhance the secretion of HCO_3^- for the calcification of shell formation; Mizuhira & Ueno (1983) in their study of the calcification of crayfish have shown that the increase of Ca^{2+}-ATPase enzymatic activities may play an important role in enhancing Ca-ion transport. However, a calcium pump has not been reported for most molluscan mantle tissue and data from the literature favour a high permeability of the outer mantle epithelium for calcium (Bielefeld *et al.*, 1993). The current study shows Ca^{2+}-ATPase enzymatic activity and the CAHase activity support the suggestion of Bielefeld *et al.* (1993) that this enzyme is involved in pH changes and dissolution of calcium salts in the intercellular space of the outer mantle epithelium.

The investigation by EDX and EFI methods of the calcifying of developing embryonic shell in *Euhadra hickonis* confirmed the role of enzymatic activities related to calcification. In *Euhadra hickonis* shell calcification takes place without calcium being supplied from external sources. With regard to the processes of calcification, we need further investigations involving autoradiographic methods using ^{45}Ca and such like, as ^{45}Ca-ion may fix well in the tissues and cells with an application of this two-step fixation method or the NHA (*N,N*-naphthaloylhydroxylamine) fixation method (Mizuhira *et al.*, 1998).

ACKNOWLEDGEMENT

We thank Professor A. C. L. Henderson, University of Stellenbosch, for reading initial drafts of this manuscript

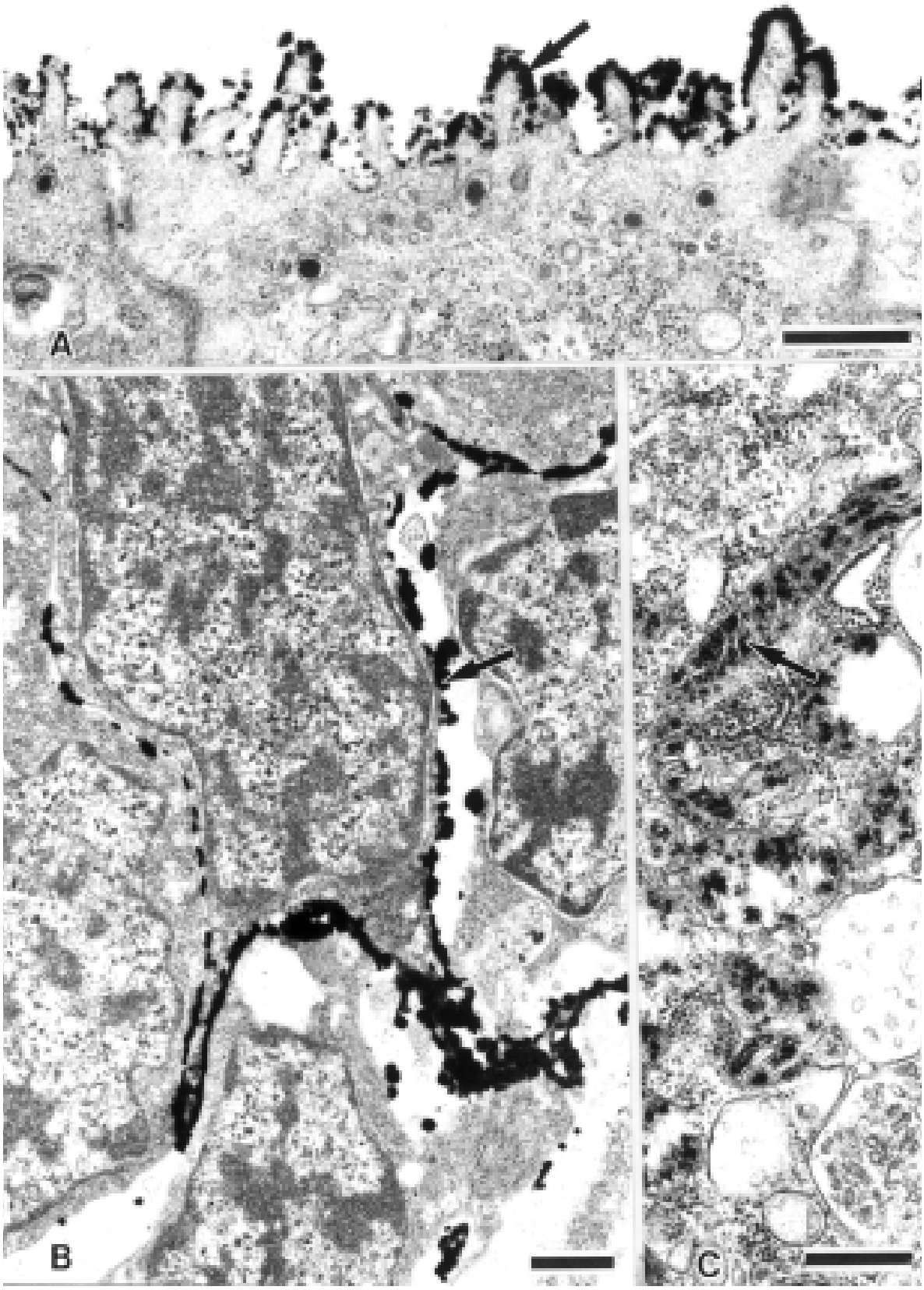

Figure 17. The localization of Ca^{2+}-ATPase. **A**. Arrow shows microvilli on the mantle epithelial cells of the day 17 and day 18 embryos. **B**. Arrow shows intercellular space of mantle epithelial cell in the day 17 and day 18 embryos. **C.** Mitochondrial cisternae in the mantle epithelial cells. Scale bars: **A** = 500 nm; **B** = 1 μm; **C** = 1 μm.

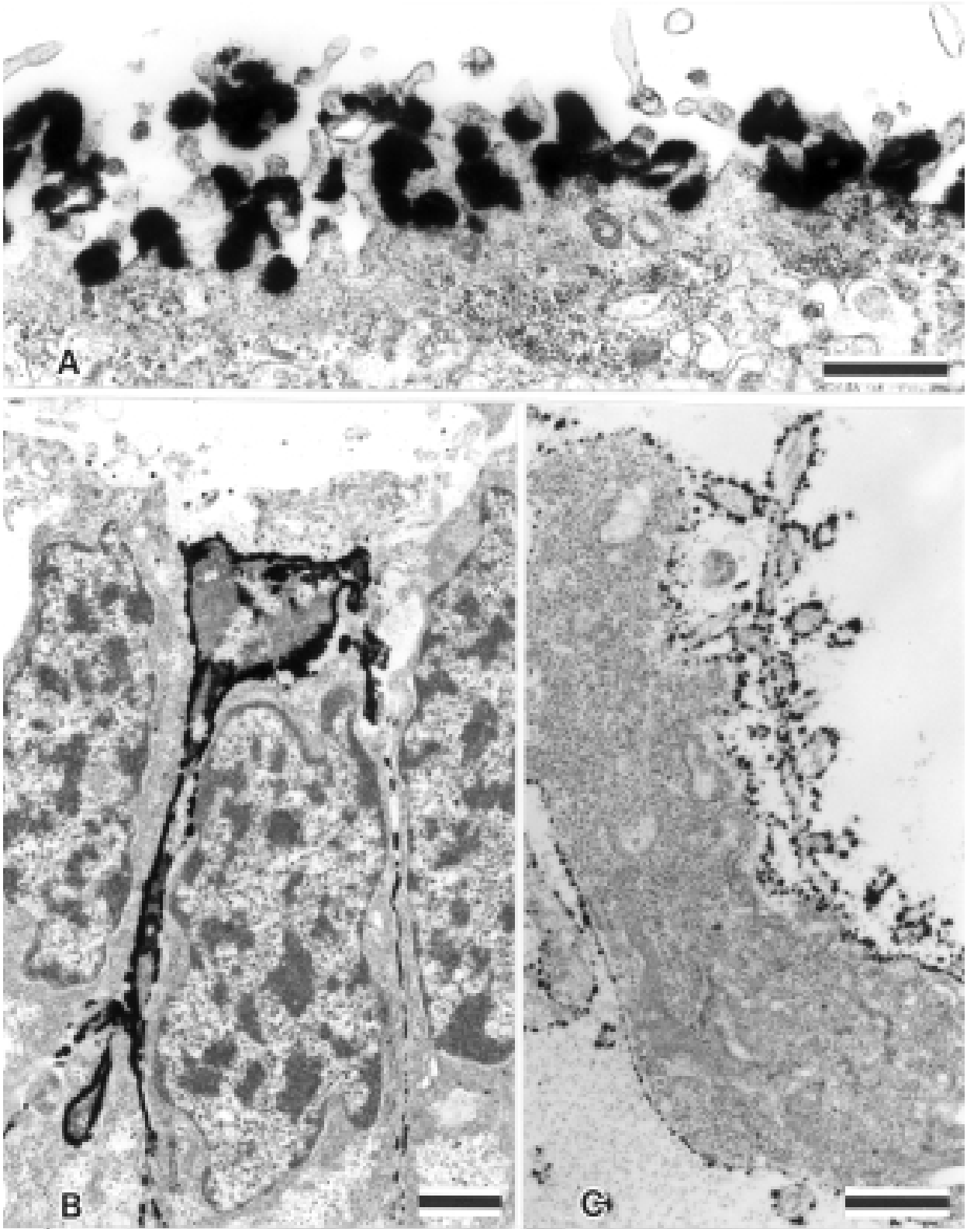

Figure 18. The localization of carbonic anhydrase (CAHase) in day 17 and day 18 *Euhadra hickonis* embryos. **A**. Microvilli in the mantle epithelial cells. **B**. Intercellular space in the mantle epithelial cells. **C**. Microvilli in the ventral epithelial cells. Scale bars: **A** = 500 nm; **B** = 1 μm; **C** = 1 μm.

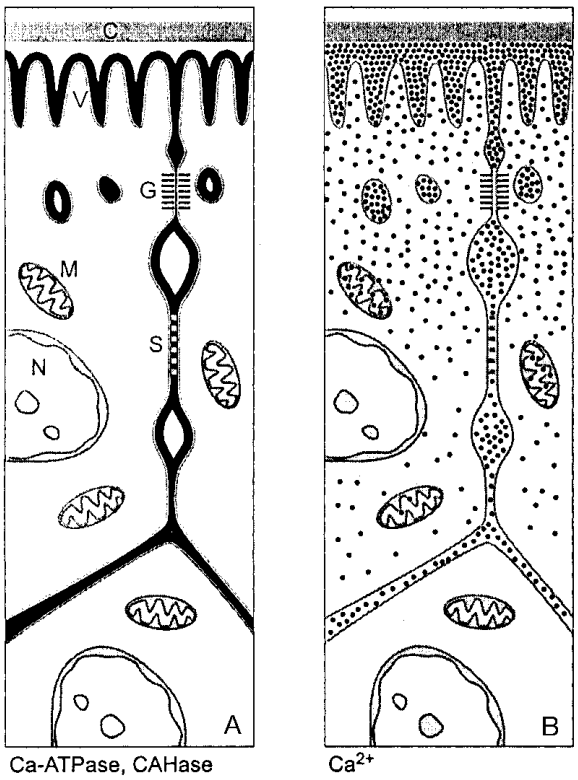

Figure 19. Schematic diagram showing the distribution of the Ca^{2+}-ATPase, CAHase enzymatic activities (**A**) and localization Ca-ion (**B**) in the day 18 and day 13 embryos, respectively. The localization of these three aspects corresponds to the same area, so there is a correlation between the transport of Ca-ion and calcification. Abbreviations: C, periostracum; V, microvilli; G, gap junction; S, septate junction; M, mitochondria; N, nucleus.

REFERENCES

ABOLINŠ-KROGIS, A. 1986. The effect of carbonic anhydrase, urea and urease on the calcium carbonate deposition in the shell-repair membrane of the snail *Helix pomatia*. *Cell and Tissue Research*, **244**: 655–660.

BANCROFT, J.D. & STEVENS, A. 1977. *Theory and practice of histological techniques*. Churchill Livingstone, Edinburgh.

BIELEFELD, U. & BECKER, W. 1991. Embryonic development of the shell in *Biomphaloria glabrata* (Say). *International Journal of Developmental Biology*, **35**: 121–131.

BIELEFELD, U., ZIEROLD, K., KORTJE, K. H. & BECKER, W. 1992. Calcium localization in the shell-fording tissue of the freshwater snail, *Biomphalaria glabrata*: a comparative study of various methods for localizing calcium. *Histochemistry Journal*, **24**: 927–938.

BIELEFELD, U., PETERS, W. & BECKER, W. 1993. Ultrastructure and cytochemistry of periostracum and mantle edge of *Biomphalaria glabrata* (Gastropoda, Basommatophora). *Acta Zoologica*, **74**: 181–193.

BOER, H.H. & WITTEVEEN, J. 1980. Ultrastructural localization of carbonic anhydrase in tissues involved in shell formation and ionic regulation in the pond snail *Lymnaea stagnalis*. *Cell and Tissue Research*, **209**: 383–390.

BORGERS, M. 1981. The role of calcium in the toxicity of the myocardium. *Histochemistry Journal*, **13**: 839–848.

BORGERS, M., DE BRABANDER, M., VAN REEMPTS, J., AWAVOTERS, F. & JACOB, W.A. 1977. Intranuclear microtubules in lung mast cells of guinea pigs in anaphylactic shock. *Laboratory Investigations*, **37**: 1–8.

BORGERS, M., THONE, F., VERHEYEN, A. & KEURS, H. 1984. Localization of calcium in skeletal and cardiac muscle. *Histochemical Journal*, **16**: 295–309.

CHETAIL, M. & KRAMPITZ, G. 1982. Calcium and skeletal structures in molluscs: concluding remarks. *Malacologia*, **22**: 337–339

EYSTER, L.S. 1983. Ultrastructure of early embryonic shell formation in the opisthobranch gastropodo *Aeolidia popillosa*. *Biological Bulletin*, **165**: 394–408.

EYSTER, L.S. 1985. Origin, morphology and fate of the nonmineralized shell of *Coryphella salmonacea*. *Marine Biology*, **85**: 67–76.

EYSTER, L.S. 1986. Shell inorganic composition and onset of shell mineralization during bivalva and gastropod embryogenesis. *Biological Bulletin*, **170**: 211–231.

FRETTER, V. & GRAHAM, A. 1962. *British prosobranch molluscs. Their functional anatomy and ecology*. Ray Society, London.

FRETTER, V. & PILKINGTON, M.C. 1971. The larval shell of some prosobranch gastropods. *Journal of the Marine Biological Association of the UK*, **51**: 49–62.

FUJIMOTO, K. & OGAWA, K. 1982. Enzyme cytochemical study of rat cardiac muscle. II. Ca^{2+}-ATPase and ouabain-sensitive, K^{+}-dependent p-nitrophenylphosphatase. *Acta Histochemistry and Cytochemistry*, 15: 338–354.

HANSSON, H.P.J. 1967. Histochemical demonstration of carbonic anhydrase activity. *Histochemistry*, **11**: 112–128.

HASSE, B., EHRENBERG, H., MARXEN, J.C., BECKER, W. & EPPLE, M. 2000. Calcium carbonate modifications in the mineralized shell of the freshwater snail *Biomphalaria glabrata*. *European Chemical Journal*, **6**: 3679–3685.

HASEGAWA, H., MIZUHIRA, V. & NOTOYA, M. 1991: A new electron staining method for ultrathin sections using microwave irradiation (MWI). *Journal of Clinical Electron Microscopy*, **24**: 864–865.

HASEGAWA, H., MIZUHIRA, V. & NOTOYA, M. 2000. Microwave-stimulated fixation and histochemical application to biological specimens. *Acta Histochemistry and Cytochemistry*, **33**: 319–340.

IRELAND, M.P. 1991. The effect of dietary calcium on growth, shell thickness and tissue calcium distribution in the snail *Achatina fulica*. *Comparative Biochemistry and Physiology, Series A*, **98**: 111–116.

IRELAND, M.P. 1993. The effect of diamox at two dietary calcium levels on growth, shell thickness and distribution of Ca, Mg, Zn, Cu, P in the tissues of the snail *Achatina fulica*. *Comparative Biochemistry and Physiology, Series C*, **104**: 21–28.

JONES, R.G. & DAVIS, W.L. 1982. Calcium-containing lysosomes in the outer mantle epithelial cells *Amblema* fresh-water mollusc. *Anatomical Record*, **203**: 337–343.

KNIPRATH, E. 1972. Formation and structure of the periostracum in *Lymnaea stagnalis*. *Cell and Tissue Research*, **9**: 260–271.

KNIPRATH, E. 1979. The functional morphology of the embryonic shell-grand in the conchiferous molluscs. *Malacologia*, **18**: 549–552.

KNIPRATH, E. 1980. Larval development of the shell and the shell-gland in *Mytilus* (Bivalvia). *Roux's Archives of Developmental Biology*, **188**: 201–204.

KNIPRATH, E. 1981. Ontogeny of the molluscan shell field: a review. *Zoologica Scripta*, **10**: 61–79.

LEGATO, M.J. & LANGER, G.A. 1969. The subcellular localization of calcium ions in mammalian myocardium. *Journal of Cell Biology*, **41**: 401.

MATA, M., STAPLE, J. & FINK, D.J. 1987. Ultrastructural distribution of Ca^{2+} with neurons. An oxalate pyroantimonate study. *Histochemistry*, **87**: 339–349.

MARXEN, J.C., HEMMER, M., GEHRKE, T. & BECKER, W. 1998. Carbohydrates of the organic shell matrix and the shell-forming tissue of the snail *Biomphalaria glabrata* (Say). *Biological Bulletin*, **194**: 231–240.

MIZUHIRA, V. 1998. Recent advances in biomedical microbeam analysis: from EDX to EELS-imaging analysis of biomedical specimens, especially with respect to calcifying tissue. *Journal of Electronic Microscopy*, **38** (suppl.): S142–146.

MIZUHIRA, V. & HASEGAWA, H. 1997. Microwave fixation and localization of calcium in synaptic terminals by means of the X-ray microanalysis (EDX) and electron energy loss spectronophy (EELS) image methods. *Brain Research Bulletin*, **43**: 53–58.

MIZUHIRA, V. & UENO, M. 1983. Calcium transport mechanism in molting crayfish revealed by microanalysis. *Journal of Histochemistry and Cytochemistry*, **31**: 214–218.

MIZUHIRA, V., HASEGAWA, H. & NOTOYA, M. 1993. Microwave fixation method for histo-cytochemistry. In: *Electron microscopic cytochemistry and immuno-cytochemistry in biomedicine* (K. Ogawa & T. Bark, eds), 17–27. CRC Press, Boca Raton.

MIZUHIRA, V., HASEGAWA, H. & NOTOYA, M. 1994. Microwave fixation and localization of calcium in synaptic vesicles. *Journal of Neuroscience Methods*, **55**: 125–136.

MIZUHIRA, V., HASEGAWA, H. & NOTOYA, M. 1997. Microwave fixation and localization of calcium in synaptic terminals and muscular cells by electron-probe X-ray microanalysis and electron energy-loss spectroscopy imaging. *Acta Histochemistry and Cytochemistry*, **30**: 277–301.

MIZUHIRA, V., HASEGAWA, H., AKAGI, T. & NAGAI, N. 1998. Demonstration of calcium ion distribution in calcifying cells X-ray microanalysis and electron spectroscopic imaging after fixation with NHA-containing fixation and microwave irradiation. *Acta Histochemistry and Cytochemistry*, **31**: 217–230.

NAKAHARA, H. & BEVELANDER, G. 1971. The formation and growth of the Prismatic layer of *Pinctada radiata. Calcified Tissue Research*, **7**: 31–45.

NOTOYA, M., HASEGAWA, H. & MIZUHIRA, V. 1990. New tissue fixation method for cytochemistry by the aid of microwave irradiation. II. Details. *Acta Histochemistry and Cytochemistry*, **23**: 525–536.

OHARA, P.T., WADA, C.R. & LIEBERMAN, A.R. 1979. Calcium storage sites in axon terminals and other components of intact C.N.S. Tissue studies with a modified pyroantimonate technique. *Journal of Autoradiography*, **129**; 869–870, 1979.

SALEUDDIN, A.S.M. 1975. An electron microscopic study on the formation of the periostracum in *Helisoma* (Mollusca). *Calcified Tissue Research*, **18**: 297–310.

SPURR, A.R. 1969. A low-viscosity epoxy resin embedding medium for electron microscopy. *Journal of Ultrastructure Research*, **26**: 31–43.

TIMMERMANS, L.P.M. 1969. Studies on shell formation in molluscs. *Netherlands Journal of Zoology*, **19**: 417–523.

WILBUR, K.M. & SALEUDDIN, A.S.M. 1983. Shell formation. In: *The Mollusca,* **4,** *Physiology Part 1* (A. S. M. Saleuddin & K. M. Wilbur, eds). Academic Press, New York.